scientific reports

Check for updates

OPEN

Proteomics analysis reveals FEN1 as a promising therapeutic target against small cell neuroendocrine carcinoma of the cervix

Jianbing Liu[1,2,6]✉, Meiying Zhong[1], Kai Yang[1], Jinjuan Wang[1], Haixia Ma[3]✉, Wei Wang[2], Lin Sun[5], Lingling Liu[4], Jing Xu[1], Xiaohua Cui[1,6], Jianqing Hao[1] & Li Li[1]

Small cell neuroendocrine carcinoma of the cervix (SCNECC) is a rare, aggressive cervical cancer with poor prognosis. This study explored molecular drivers of SCNECC progression and identified potential therapeutic targets. Proteomic analysis was conducted to identify differentially expressed proteins (DEPs) in SCNECC. Subsequent GO and KEGG enrichment analyses were performed to delineate key DEPs. Functional assays, including CCK-8, colony formation, cell cycle, and apoptosis assays, were conducted to assess the roles of target genes. Expression levels of target genes were validated using qRT-PCR, western blot, and immunohistochemistry (IHC). Proteomic profiling revealed 2333 DEPs in SCNECC, comprising 2168 upregulated and 165 downregulated proteins. GO and KEGG analyses revealed that the upregulated DEPs were predominantly enriched in processes occurring within the cell nucleus, such as DNA replication, reflecting heightened proliferative activity in SCNECC. IHC confirmed FEN1 overexpression. Functional assays showed that FEN1 knockdown suppressed cell viability, colony formation, and cell cycle, promoted apoptosis, and impeded tumor growth in mice. SC13, a FEN1 inhibitor, also had similar effects. Furthermore, silencing FEN1 markedly reduced PIK3CA, PCNA, and BCL-2 levels, while elevating Caspase-9 expression. CONCLUSION: FEN1 overexpression fuels SCNECC progression via PCNA regulation, positioning FEN1 as a promising SCNECC therapeutic target.

Keywords Small cell neuroendocrine carcinoma of the cervix (SCNECC), Proteomic profiling, FEN1 protein, Therapeutic target

Abbreviations

PCR	Polymerase chain reaction
WB	Western blot
NC	Negative control
SCNECC	Small cell neuroendocrine carcinoma of the cervix
FEN1	Flap structure-specific endonuclease 1
DEP	Differentially expressed protein
PCNA	Proliferating cell nuclear antigen
PBS	Phosphate buffered saline
HPV	Human papilloma virus

Cervical cancer is the fourth commonly diagnosed cancer (6.8% of 9.7 million new cases) and the fourth leading cause of cancer death (8.1% of 4.3 million deaths) in women all over the world[1] and especially among women aged 30 to 44, the incidence rates increased by 1–2% annually[2]. Small cell neuroendocrine carcinoma of the cervix (SCNECC) represents an exceptionally rare subtype of cervical malignancy, comprising less than 1.0% of

[1]School of Basic Medical Sciences, Key Laboratory of Cellular Physiology(Shanxi Medical University, Ministry of Education), Shanxi Medical University, Taiyuan 030001, China. [2]Departments of Obstetrics and Gynecology, the Second Hospital of Shanxi Medical University, Taiyuan 036000, China. [3]Department of Pathology, Shanxi Province Cancer Hospital, Taiyuan 030013, China. [4]Pathology Department, Third Hospital of Shanxi Medical University, Taiyuan 030032, China. [5]Shanxi Second People's Hospital, General Surgery Department, Taiyuan 030012, China. [6]Shanxi Key Laboratory of Functional Proteins, Shanxi Medical University, Taiyuan 030001, China. ✉email: liujianbing@sxmu.edu.cn; 756985520@qq.com

all cervical cancers[3]. SCNECC is characterized by a markedly aggressive phenotype and an elevated propensity for rapid metastasis compared to other cervical cancer variants[4]. In the treatment of SCNECC, the traditional approaches such as surgery, radiotherapy and chemotherapy are mainly employed, and currently surgery has relatively good therapeutic effects[3]. However, 3- and 5-year overall survival rates of SCNECC were only around 36.2% and 30.6%, respectively[5,6] which reflects that the overall treatment effect is not very ideal, and new treatment approach still needs to be further explored.

With the advancement of science and technology, a variety of cancer treatment methods with fewer side effects and higher efficacy have been researched and applied in clinical treatment, including photodynamic therapy, targeted therapy, antibody drug conjugates, and chimeric antigen receptor T cell therapy, etc[7]. Especially, the advent of targeted therapies resulted in significant improvement in cancer treatment efficacy, increases in remissions duration, decreases in treatment toxicities, and marked by decreases in cancer mortality[7]. In targeted therapy, you can design drugs to target stromal cells and/or immune cells in the tumor microenvironment, thereby inhibiting the malignant progression of tumor cells, as they have established a symbiotic relationship that can alter the course of the tumor[8]. However, targeting tumor cells directly can be more effective and precise in inhibiting the progression of tumors, and even killing them[9]. For example, trastuzumab, which targets ERBB2, is the first drug for targeted cancer treatment[10]. Targeted therapy is expected to be combined with traditional treatment regimens to enhance the therapeutic effect of SCNECC and improve the prognosis of patients[11]. However, up to now, there are no specific targeted drugs for SCNECC. Therefore, this study aims to explore the targets for targeted therapy of SCNECC, providing a scientific basis for the development of targeted drugs.

The application of "omics-based" technologies in malignancy will offer fresh insights into the molecular underpinnings of cancer, facilitate early detection, prognosis, and population-wide screening, and assess therapeutic responses while fostering the development of innovative therapeutic strategies[11–14]. Proteomics, the large-scale examination of protein attributes including expression levels, post-translational modifications, and protein-protein interactions, is instrumental in gaining a holistic understanding of diseases at the protein level. By comparing the protein profiles of cancer tissues with those of adjacent tissues, specific "disease-specific protein molecules" can be identified, serving as molecular targets for drug design or as biomarkers for early disease diagnosis[15,16]. Certain scholars had endeavored to pinpoint novel targets for the targeted therapy of SCNECC by conducting proteomic analyses, subsequently proposing CDN2A and SYP as potential therapeutic candidates[12]. This study drew upon proteomic research specific to SCNECC, uncovering a marked overexpression of flap structure-specific endonuclease 1 (FEN1) within the cancerous tissues of SCNECC. Furthermore, the experimental data proved that the FEN1 overexpression significantly promoted the progression of SCNECC. Ultimately, the application of an FEN1 inhibitor provided additional evidence, reinforcing the potential of FEN1 as a viable and targeted therapeutic candidate.

Results

Baseline characteristics of patients with SCNECC

A total of 6 cases of SCNECC with comprehensive clinical pathological records were selected for analysis. Among these cases, there were 5 tumors classified as stage IB (comprising 1 case of stage IB1, 3 cases of stage IB2, and 1 case of stage IB3) and 1 tumor classified as stage II (specifically, stage IIA2). High-risk human papillomavirus (HPV) testing indicated that all six patients were positive for HPV 18 infection. Notably, lymph node metastasis was observed in three of these patients. A detailed breakdown of the patients' characteristics is provided in Table 1.

To identify DEPs in SCNECC, we initially employed immunohistochemical techniques to assess the expression levels of key marker proteins, namely cytokeratin AE1/AE3, synaptophysin (SYN, a neuroendocrine marker), Ki67 (a proliferation marker), and P16 (a diagnostic marker for cervical cancer). The experimental findings revealed that the staining intensities of AE1/AE3, SYN, Ki67, and P16 were notably more intense in cancerous tissues compared to adjacent non-cancerous tissues (Fig. 1A). A scoring analysis of the staining intensities further indicated that the scores for AE1/AE3, SYN, Ki67, and P16 in cancerous tissues were 6, 6.3, 6, and 9, respectively, whereas the corresponding scores in adjacent non-cancerous tissues were 1.02, 0.68, 0.67, and 1.04 (Fig. 1B). The findings indicate a notable increase in the expression levels of AE1/AE3, SYN, Ki67, and P16 in SCNECC when compared to adjacent non-cancerous tissues.

Proteomic screening of DEPs in SCNECC

To gain deeper insights into the molecular changes associated with SCNECC, we conducted a proteomic comparative analysis of cancerous and adjacent non-cancerous tissue samples from the six SCNECC patients (Table 1). Using $|FC| \geq 1.5$ and $P < 0.05$ as cut-offs[17] we identified 2333 proteins that were differentially expressed

Pathology number	Age	Tumor size (Length * width * height)	Lymphatic metastasis	HPV infection	FIGO
2017–05687	26	2.2*1.7*1 cm^3	No	HPV18 (+)	IB2
2017–06658	43	5*5*3 cm^3	No	HPV18 (+)	IB3
2020–06749	51	1.5*1.5*1 cm^3	No	HPV18 (+)	IB1
2013–09135	46	4.5*3*2.5 cm^3	Yes	HPV18 (+)	IIA2
2018–02851	34	5*4*3 cm^3	Yes	HPV18 (+)	IB2
2019–09378	47	3.5*3*1.5 cm^3	Yes	HPV18 (+)	IB2

Table 1. Pathological information of the six patients with SCNECC in this study.
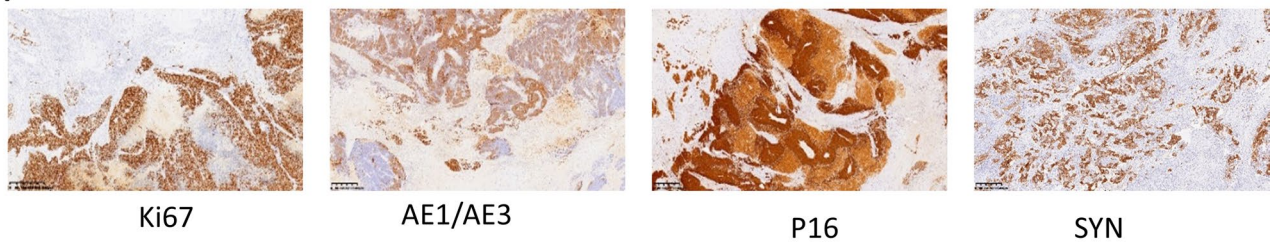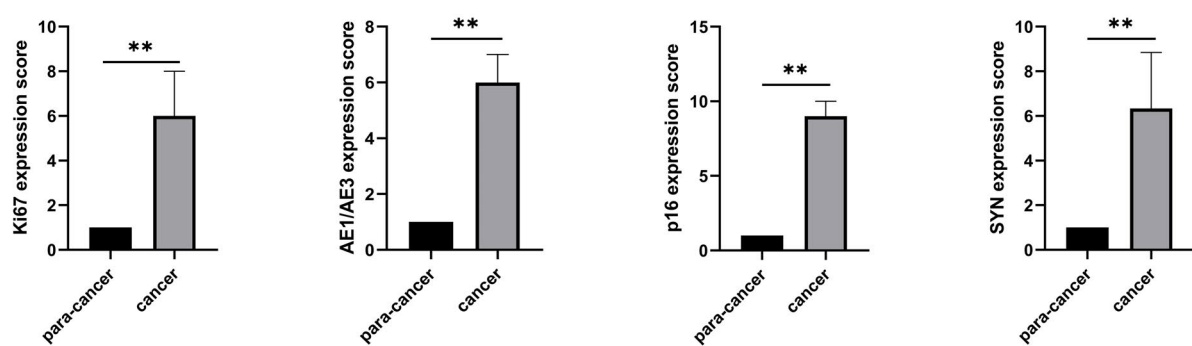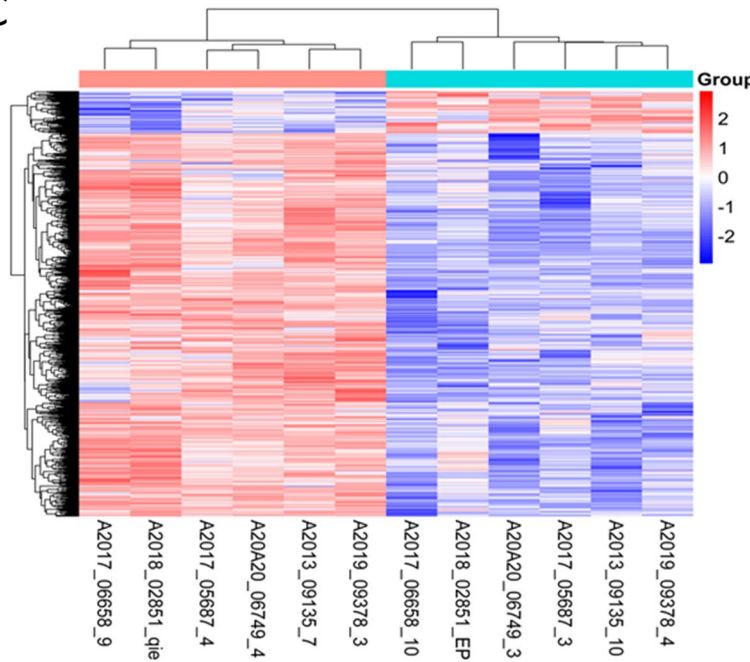
Fig. 1. Proteomic Analysis of DEPs in SCNECC. **A**. Immunohistochemical analysis of Ki67, AE1/AE3, P16 and SYN expression levels in SCNECC tissues and adjacent non-cancerous tissues. **B**. The expression scores of Ki67, AE1/AE3, P16 and SYN in SCNECC tissues are compared with those in adjacent non-cancerous tissues. Two-independent-samples t-tests was employed to analyze the experimental data. Statistical significance is indicated as follows: * for $P < 0.05$, indicating a significant difference; ** for $P < 0.01$, indicating a highly significant difference. **C**. This heatmap depicts the DEPs in SCNECC, as identified by proteomic analysis. Proteins were selected based on the criteria of |FC| > 1.5 and $P < 0.05$. Red color represents up-regulated proteins, while blue color represents down-regulated proteins.

in SCNECC. Specifically, 2168 proteins were upregulated, and 165 proteins were downregulated in cancerous tissues compared to adjacent non-cancerous tissues (Fig. 1C, Supplementary Table 1).

Gene ontology (GO) and Kyoto encyclopedia of genes and genomes (KEGG) analysis of DEPs in SCNECC

To elucidate the proteomic expression signatures of SCNECC, we performed separate GO analyses for DEPs categorized as up-regulated and down-regulated. For up-regulated DEPs, biological process (BP) annotations were predominantly enriched in mRNA splicing pathways, including mRNA splicing, RNA splicing, mRNA processing, translational initiation, and nuclear-transcribed mRNA catabolic processes (Fig. 2A). Cellular component (CC) analysis highlighted their localization primarily in the nucleus, nucleoplasm, membrane, nucleolus, and nuclear speckles (Fig. 2A). Molecular function (MF) terms were largely associated with RNA binding, DNA binding, mRNA binding, nucleic acid binding, and hydrolase activity (Fig. 2A). In contrast, down-regulated DEPs exhibited distinct enrichment patterns. BP terms were primarily involved in extracellular matrix (ECM) organization, platelet degranulation, collagen fibril organization, cornification, and negative regulation of endopeptidase activity (Fig. 2B). CC analysis revealed significant enrichment in extracellular exosomes, extracellular space, extracellular regions, collagen-containing ECMs, and blood microparticles (Fig. 2B). MF terms were strongly linked to heparin binding, signaling receptor binding, serine-type endopeptidase inhibitor activity, ECM structural constituents, and cytoskeletal structural components (Fig. 2B). Subsequently, we conducted KEGG pathway enrichment analysis to identify critical pathways associated with SCNECC. Up-regulated DEPs showed prominent enrichment in spliceosome assembly, RNA transport, DNA replication, base excision repair, and ribosomal biogenesis (Fig. 3A). Conversely, down-regulated DEPs were significantly enriched in complement and coagulation cascades, proteoglycan signaling in cancer, vascular smooth muscle contraction, vitamin digestion and absorption, and cholesterol metabolism (Fig. 3B).

Based on the integrated GO and KEGG analyses, DEPs in SCNECC are primarily enriched in cellular events and signaling pathways related to DNA replication and RNA transcription. Notably, FEN1 (Flap endonuclease 1) was enriched in DNA replication and base excision repair pathways within the KEGG analysis, underscoring its role in DNA repair and genomic stability maintenance (Supplementary Table 2). Proteomic profiling revealed a 17-fold increase in FEN1 expression in cancerous tissues compared to adjacent non-cancerous tissues (Supplementary Table 1).

### Overexpressed FEN1 modulates PCNA in SCNECC

To validate the expression level of FEN1 in SCNECC, we employed immunohistochemical (IHC) and observed that the staining intensity of FEN1 was significantly more intense in cancerous tissues compared to adjacent non-cancerous (para-cancer) tissues (Fig. 4A). Notably, the mean staining score for cancerous tissues was 8, in stark contrast to a score of only 1 for adjacent non-cancerous tissues, highlighting a statistically significant difference (Fig. 4B). To elucidate the underlying mechanism of FEN1, we searched for FEN1 in the STRING database and obtained its interaction network, wherein FEN1 and PCNA were both expressed and exhibited the highest combined score (Fig. 4C, Supplementary Table 3). Additionally, PCNA was identified as a differentially expressed protein in SCNECC and was enriched in the DNA replication pathway of KEGG signaling pathways (Supplementary Table 2).

To investigate the role of FEN1 in the pathogenesis and progression of SCNECC, we initially established a cell model with reduced FEN1 expression using gene silencing technology. In TC-YIK cells, transfection with either NC or FEN1 siRNA was performed. Compared to the NC group, Quantitative reverse transcription PCR (qRT-PCR) confirmed a substantial reduction in FEN1 mRNA levels in the FEN1 siRNA group (Fig. 4D), and Western blot (WB) analysis demonstrated a significant decrease in FEN1 protein levels in the FEN1 siRNA group (Fig. 4E). Furthermore, when FEN1 was knocked down by transfecting with FEN1 siRNA in the TC-YIK cell lines, both the mRNA and protein levels of PCNA were significantly reduced compared to the NC group (Fig. 4D, E).

### FEN1/PCNA enhances proliferation and blocks apoptosis in TC-YIK cells

In the study of the function of FEN1/PCNA in SCNECC, the results from the Cell Counting Kit-8 assay (CCK-8) assay indicated that, compared to the NC group, the proliferation activity of the FEN1 siRNA group was significantly lower at 48 h post-transfection, with this difference becoming even more pronounced at 72 h; the cell viability of the PCNA siRNA group was also notably inhibited at 72 h (Fig. 5A). Flow cytometry analysis revealed that, relative to the NC group, the apoptosis rate of TC-YIK cells significantly increased after FEN1 knockdown, and there was also a marked increase in the number of cells entering apoptosis in the PCNA siRNA group (Fig. 5B).The colony formation assay demonstrated that, compared to the NC group, the number of colonies formed by the FEN1 siRNA group was significantly reduced, showing statistical significance, and there was also a substantial decrease in the number of cell colonies in the PCNA siRNA group (Fig. 5C). Furthermore, although the proportion of cells in the G0/G1 phase did not show significant changes in the FEN1 siRNA group, the percentages of cells in the S phase and G2/M phase were notably decreased (Fig. 5D). Additionally, the proportion of cells in the G0/G1 phase increased significantly in the PCNA siRNA group, while the percentage of cells in the S phase decreased significantly, with no substantial change observed in the G2/M phase (Fig. 5D).

To further substantiate the effects of FEN1 knockdown on the biological functions of TC-YIK cells at the molecular level, we examined the expression changes of several pivotal genes associated with cellular biology. After transfecting TC-YIK cells with either NC or *FEN1* siRNA, qRT-PCR results at 24 h demonstrated that, compared to the NC group, the mRNA levels of *BCL-2* and *PIK3CA* were significantly reduced, whereas the mRNA level of *Caspase-9* was significantly elevated in the FEN1 siRNA group (Fig. 5E). At 48 h, WB analysis
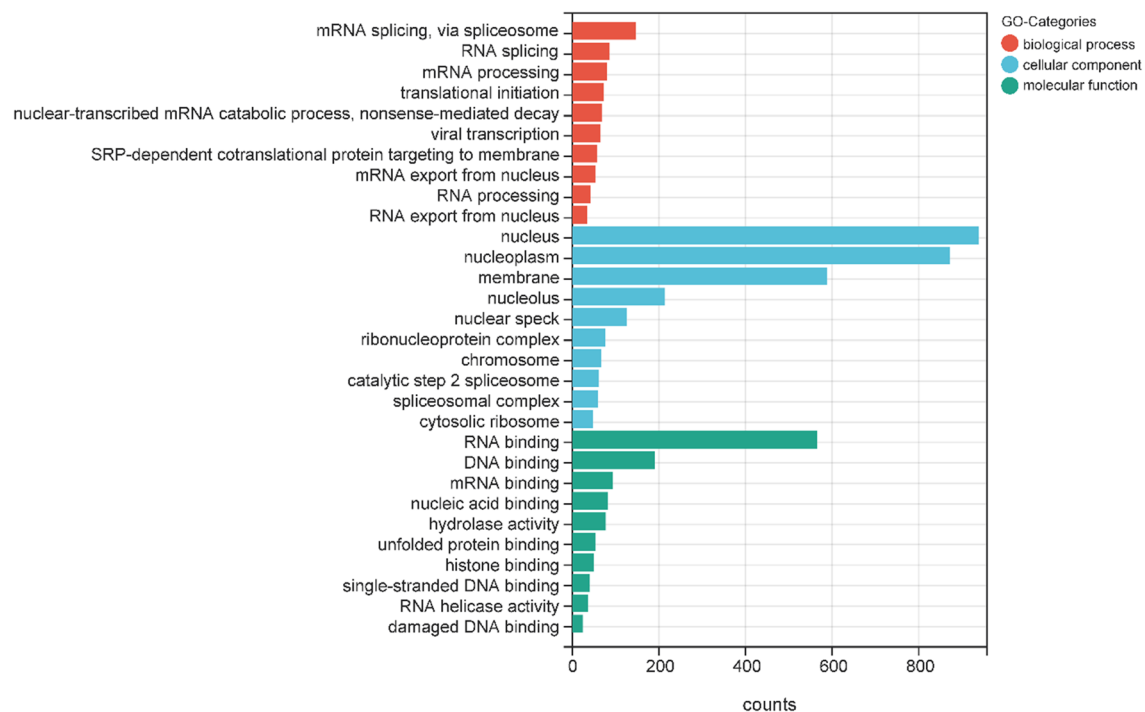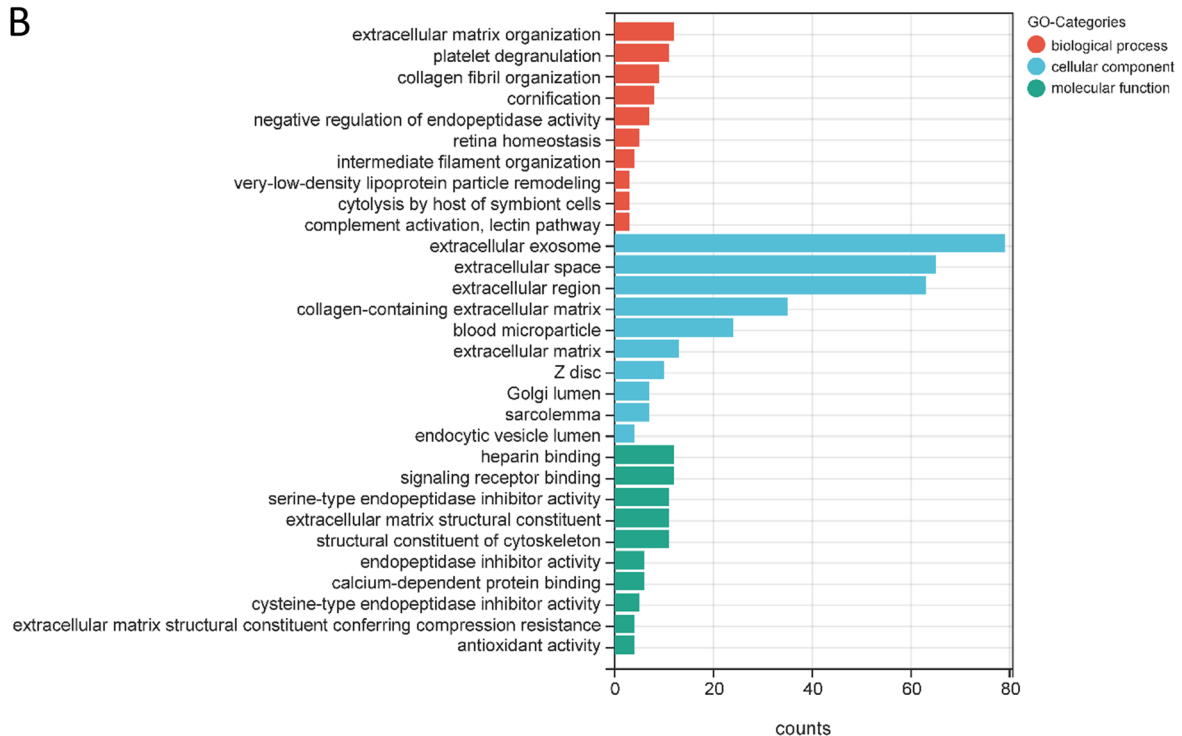
Fig. 2. GO analysis of the up- and down-regulated proteins in SCNECC. **A** GO enrichment analysis for up-regulated proteins. **B** GO enrichment analysis for down-regulated proteins. The Y-axis represents the GO terms, and X-axis represents the number of DEPs annotated in this GO terms.
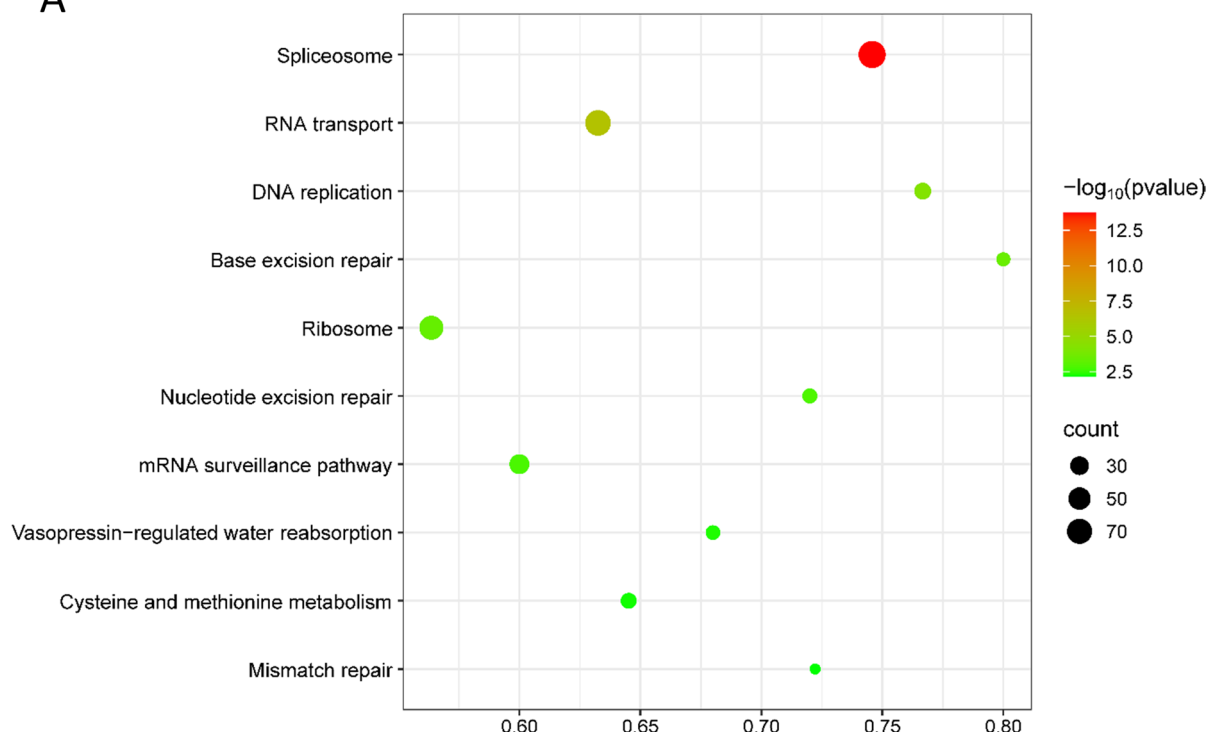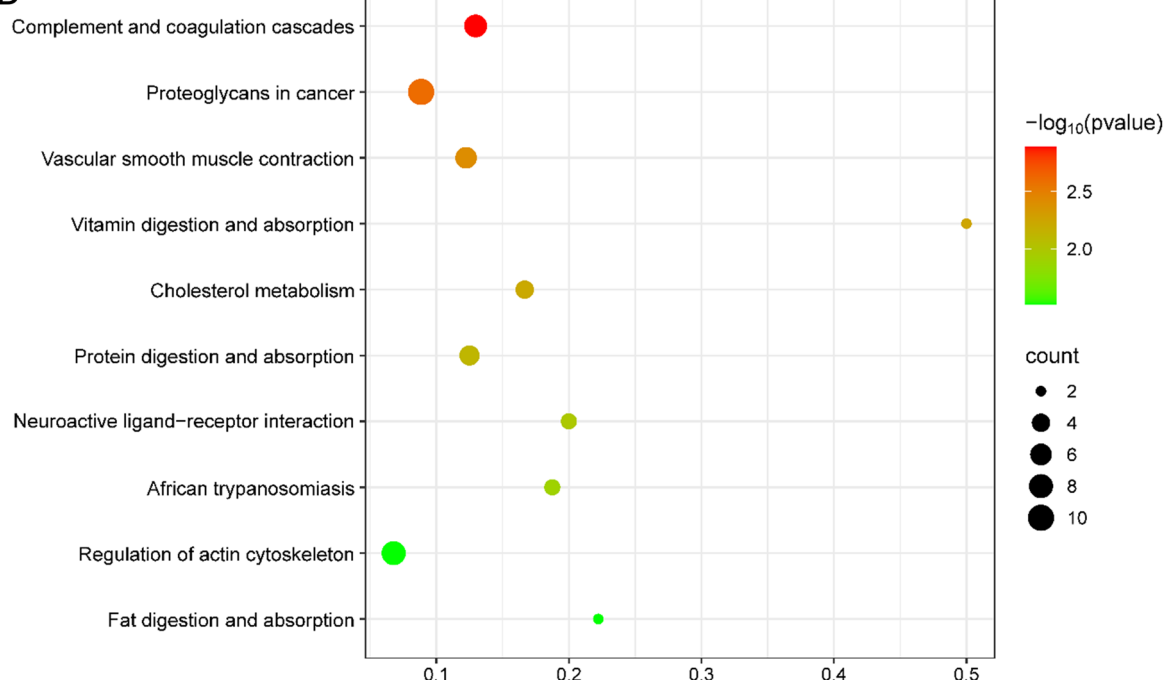
Fig. 3. KEGG analysis of the up- and down-regulated proteins in SCNECC. **A.** KEGG enrichment analysis for up-regulated proteins. **B.** KEGG enrichment analysis for down-regulated proteins. The Y-axis denotes the KEGG pathway, while the X-axis represents the ratio of DEPs to the total number of proteins annotated within each pathway. The coloration of the dots corresponds to the significance level of the adjusted p-value, and the size of the circular markers is scaled to reflect the quantitative abundance of DEPs identified in each pathway.
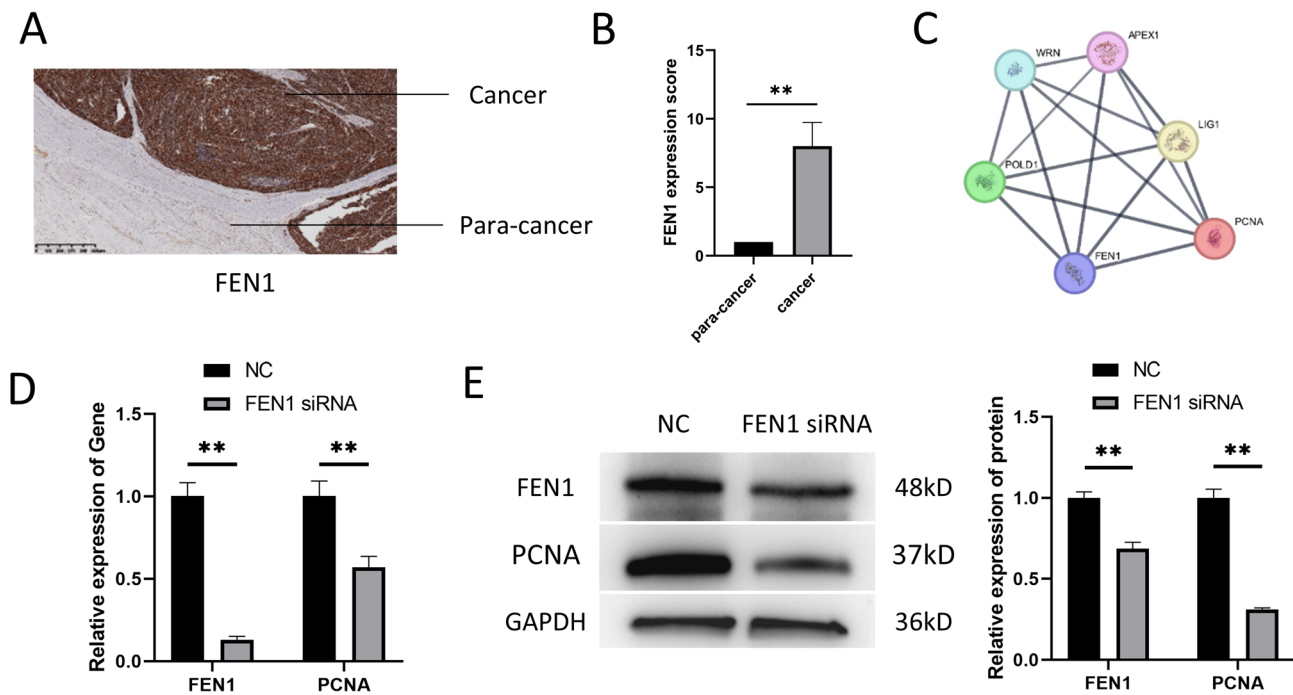
Fig. 4. The expression of FEN1 and the regulation of *FEN1* on PCNA in SCNECC. **A** Immunohistochemical detection and expression analysis of FEN1 in SCNECC. **B** Expression levels were scored and analyzed, with statistical significance indicated by asterisks compared to adjacent non-cancerous tissues. **C** The interaction network of FEN1 was obtained from the STRING database. **D** TC-YIK cells were transfected with either negative control (NC) siRNA or *FEN1*-specific siRNA for 24 h. Relative mRNA expression levels of *FEN1* and *PCNA* were detected by qRT-PCR, with *GAPDH* serving as the internal reference gene. $n = 3$. **E** Following transfection of TC-YIK cells with NC or *FEN1* siRNA for 48 h, protein expression levels of FEN1 and PCNA were examined by WB analysis. Grayscale analysis and statistical evaluation of the WB results were performed using ImageJ software. Two-independent-samples t-tests was employed to analyze the experimental data.

confirmed that the protein levels of BCL-2 and PIK3CA were significantly decreased, while the protein expression of Caspase-9 was markedly increased in the FEN1 siRNA group (Fig. 5F).

FEN1 knockdown inhibits tumor growth in TC-YIK xenograft models

To explore the impact of FEN1 knockdown on tumor growth in vivo, we initially subcutaneously injected TC-YIK cells into nude mice to initiate tumor development. Upon the tumors reaching a volume of approximately 50 mm³, the mice were administered either in vivo NC or in vivo FEN1 siRNA (Fig. 6A). The findings revealed that, in contrast to the in vivo NC group, the body weight of mice in the in vivo FEN1 siRNA group exhibited no significant alteration (Fig. 6B). Notably, the tumor weight was significantly reduced in the in vivo FEN1 siRNA group (Fig. 6C, D), and the tumor volume was also considerably smaller (Fig. 6E).

When compared to the in vivo NC group, the mRNA expression levels of *FEN1*, *PCNA*, *BCL-2* and *PIK3CA* were significantly diminished, whereas the mRNA level of *Caspase-9* was significantly elevated in the in vivo FEN1 siRNA group (Fig. 6F). Moreover, the protein levels of FEN1, PCNA, BCL-2, and PIK3CA were also markedly decreased, while the protein level of Caspase-9 was significantly increased in the in vivo FEN1 siRNA group (Fig. 6G).

FEN1 inhibitor SC13 hinders TC-YIK cell growth

To determine whether a pharmacological inhibitor of *FEN1* can hinder the development of SCNECC, we exposed TC-YIK cells to SC13, a *FEN1* inhibitor, and assessed alterations in the biological behaviors of these cells. In comparison to the control group (SC13 0 µM), treatment with SC13 resulted in a significant reduction in the viability of TC-YIK cells at 48 h and 72 h (Fig. 7A). Additionally, it induced a notable increase in the apoptosis of TC-YIK cells (Fig. 7B). SC13 also led to a substantial decrease in the number of TC-YIK cell colonies (Fig. 7C). Regarding the cell cycle phases, there were no significant changes observed in the proportions of cells in the G0/G1 and S phases; however, the proportion of cells in the G2/M phase decreased (Fig. 7D). qRT-PCR experiments revealed that, compared to the control group, treatment with SC13 for 24 h significantly reduced the mRNA levels of *FEN1*, *PCNA*, *BCL-2*, and *PIK3CA* in TC-YIK cells, while increasing the mRNA level of the Caspase-9 gene (Fig. 7E). Furthermore, WB experiments confirmed that, compared to the control group, treatment with SC13 for 48 h significantly decreased the protein levels of FEN1, PCNA, BCL-2 and PIK3CA in TC-YIK cells, while enhancing the protein expression of the *Caspase-9* gene (Fig. 7F).
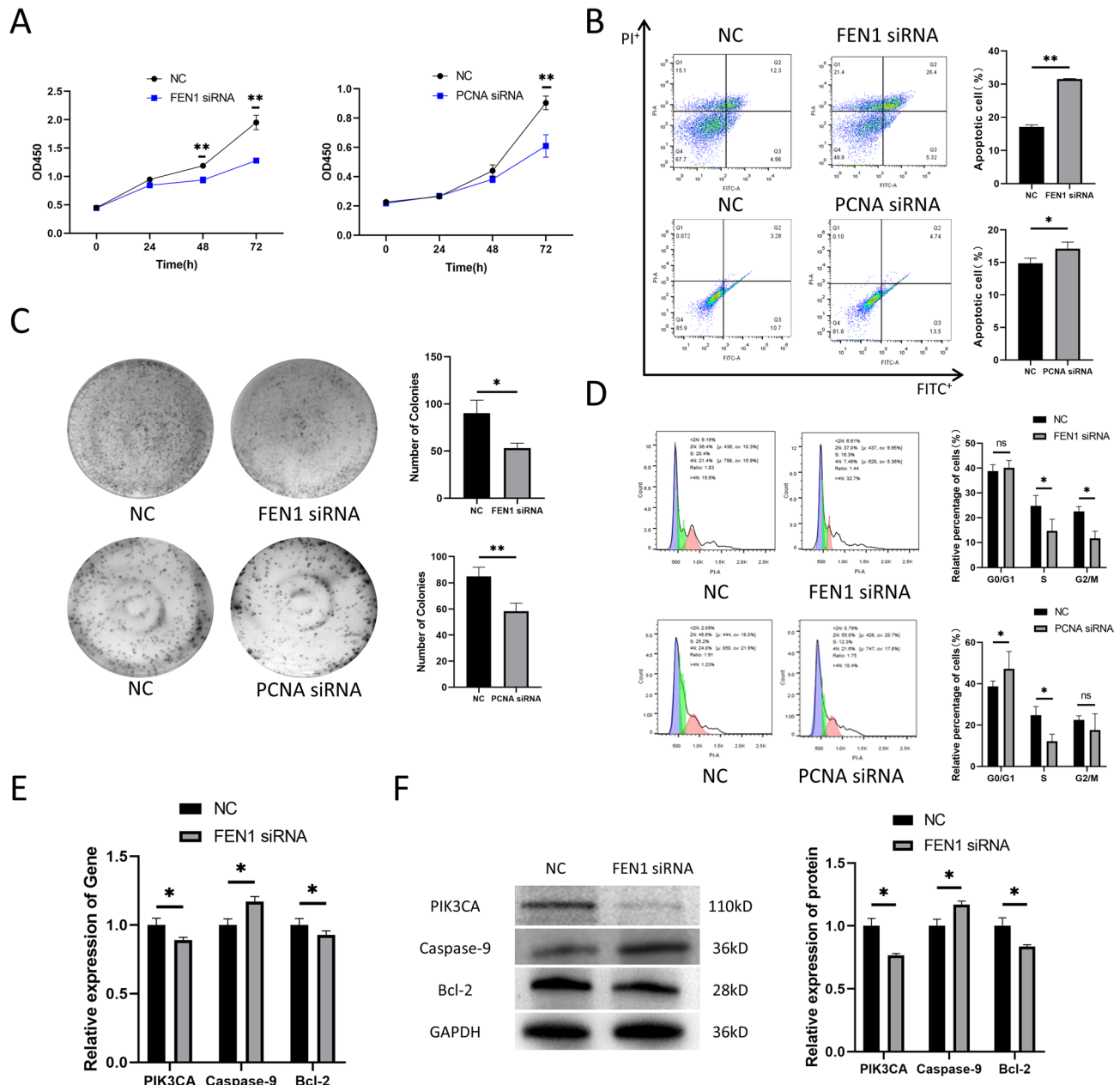
Fig. 5. The role of FEN1/PCNA in TC-YIK Cells. (**A**) After transfecting TC-YIK cells with NC, *FEN1* siRNA or *PCNA* siRNA, cell proliferation activity was assessed at 0 h, 24 h, 48 h and 72 h using the CCK-8 method, and statistical analysis was conducted. $n = 5$. ANOVA was employed to analyze the experimental data. (**B**) Apoptosis was detected using flow cytometry 48 h post-transfection, and the results were statistically analyzed. $n = 3$. (**C**) Colony formation assay and quantitative analysis of colony numbers using crystal violet staining, $n = 3$. (**D**) Cell cycle changes were analyzed by flow cytometry 48 h after transfection, and statistical analysis of the results was performed. $n = 3$. (**E**) After transfecting TC-YIK cells with NC or *FEN1* siRNA for 24 h, qRT-PCR was performed to determine the relative mRNA expression levels of *BCL-2*, *PIK3CA*, and *Caspase-9*, using *GAPDH* as the internal reference gene. $n = 3$. (**F**) WB analysis was conducted to examine the protein expression levels of BCL-2, PIK3CA, and Caspase-9 in TC-YIK cells 48 h after transfection with NC or *FEN1* siRNA. Grayscale analysis and statistical evaluation of the WB bands from Panel F were performed using ImageJ software. Data are presented as means ± SDs. Comparisons with the NC group: *: $P < 0.05$; **: $P < 0.01$. Two-independent-samples t-tests was employed to analyze the experimental data in B-F.
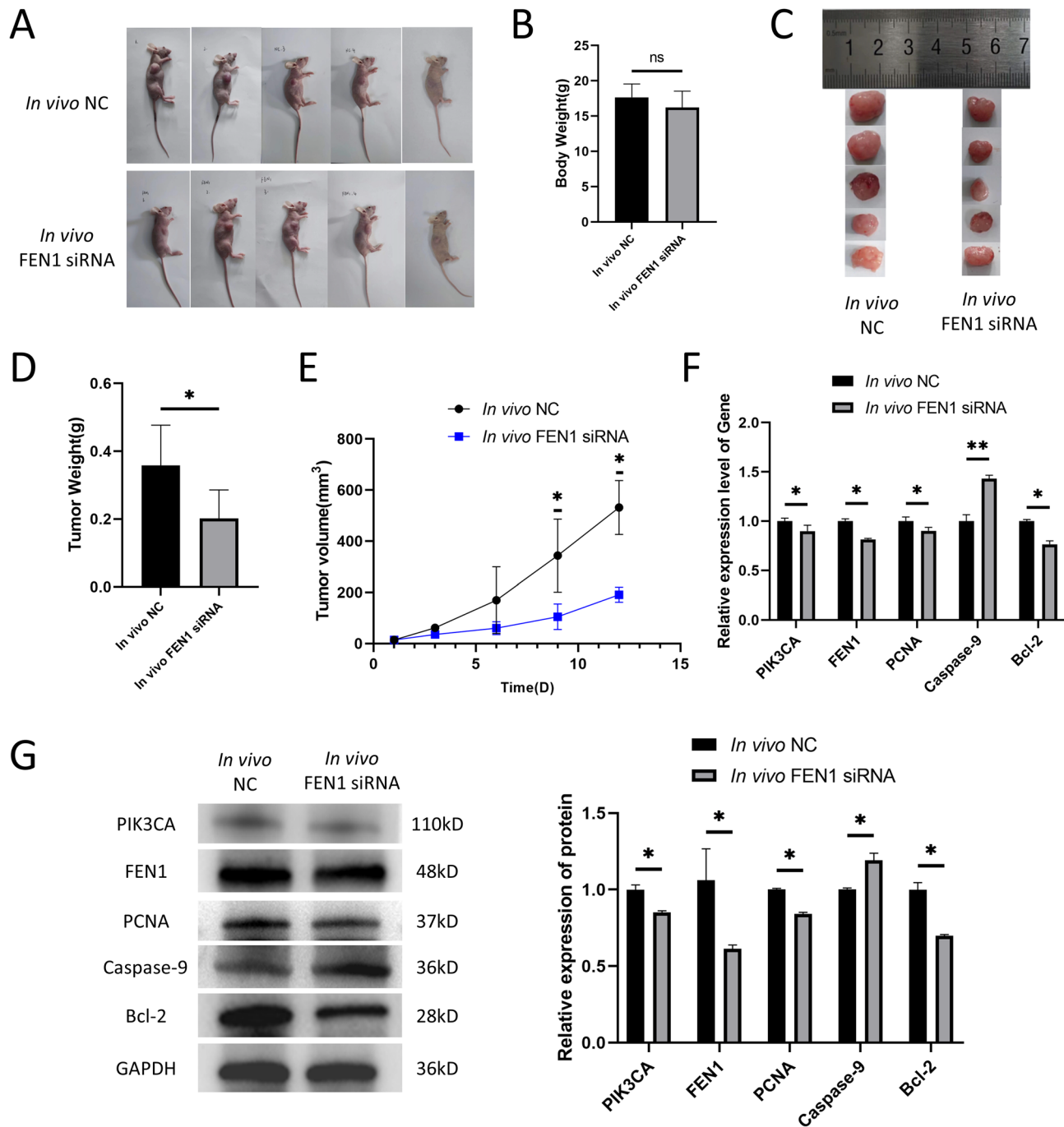
Fig. 6. In Vivo Assessment of the Effect of *FEN1* Knockdown on Tumor Growth in SCNECC Xenografts. **A** Representative images of tumor-bearing nude mice from the in vivo NC siRNA group and the *in vivo FEN1* siRNA group. **B** Comparison of body weights of nude mice with tumors in the in vivo NC group and the *in vivo FEN1* siRNA group. **C** Excised tumor samples from nude mice in the in vivo NC group and the *in vivo FEN1* siRNA group. **D** Comparison of tumor weights from nude mice in the in vivo NC group and the *in vivo FEN1* siRNA group. **E** Comparison of tumor volumes in nude mice from the in vivo NC group and the *in vivo FEN1* siRNA group. ANOVA was employed to analyze the experimental data. **F** qRT-PCR was performed to detect the relative mRNA expression levels of *FEN1*, *PCNA*, *BCL-2*, *PIK3CA*, and *Caspase-9* in the SCNECC xenografts, using *GAPDH* as the internal reference gene. $n = 3$. **G** The relative protein expression levels of FEN1, PCNA, BCL-2, PIK3CA, and Caspase-9 were examined by WB analysis in the SCNECC xenografts, using GAPDH as the internal reference gene. $n = 3$. Grayscale analysis and statistical evaluation of the WB bands were performed using ImageJ software. Compared to the in vivo NC group, ns: $P > 0.05$ indicates no statistical significance, *: $P < 0.05$ indicates statistical significance, while **: $P < 0.01$ indicates high statistical significance. Two-independent-samples t-tests was employed to analyze the experimental data in the B, D, F, and G.
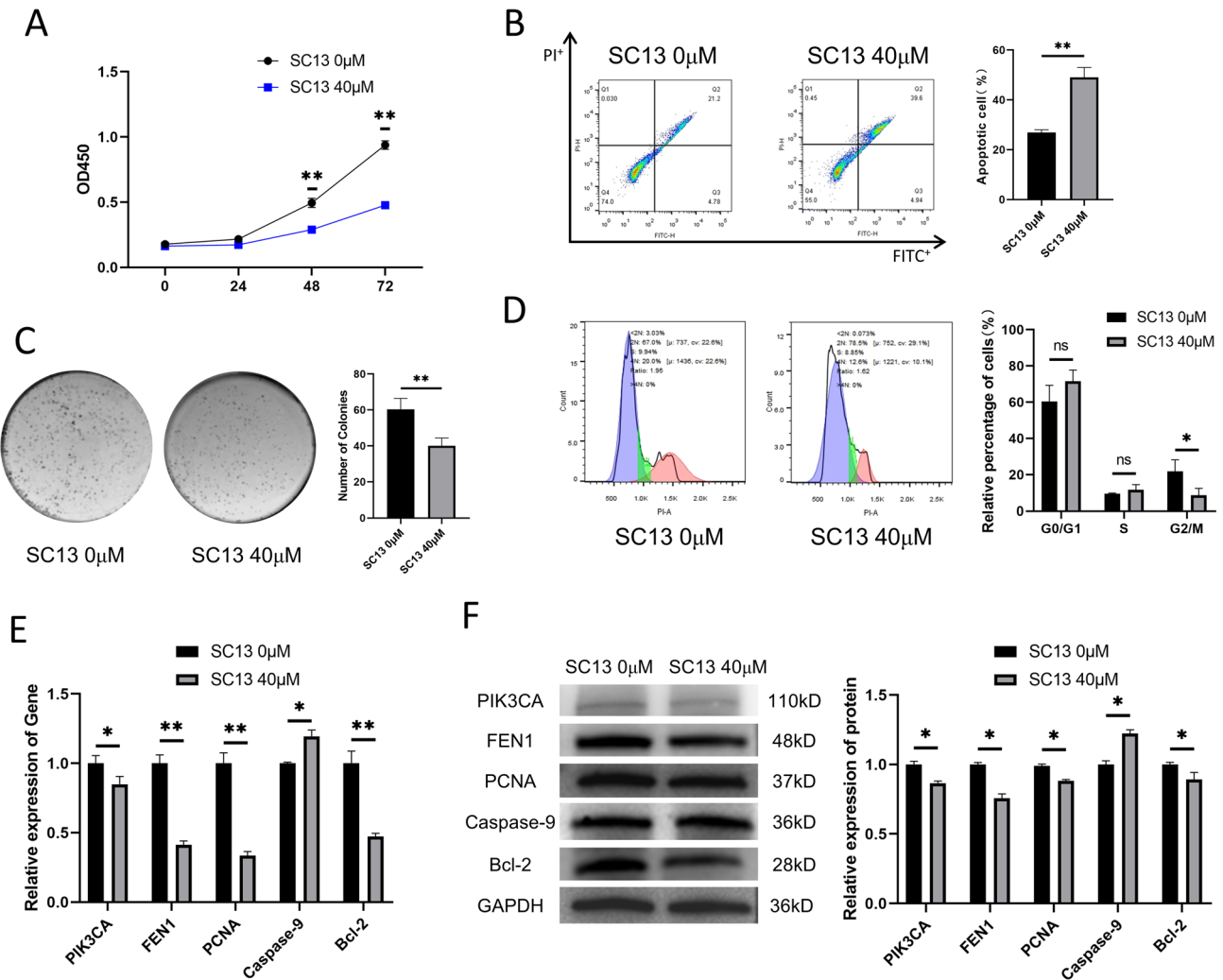
Fig. 7. Effects of FEN1 Inhibitor SC13 on Clonogenic Capacity, Proliferation, Apoptosis, and Cell Cycle of TC-YIK Cells.

After treatment with the SC13 inhibitor in TC-YIK cells, the following assessments were performed: (**A**) Cell proliferation activity was measured using the CCK-8 assay at 0 h, 24 h, 48 h and 72 h, followed by statistical analysis. $n = 5$. ANOVA was employed to analyze the experimental data. (**B**) Flow cytometry was used to detect apoptosis 48 h after SC13 inhibitor treatment, with subsequent statistical analysis. $n = 3$. (**C**) Colony formation was visualized by crystal violet staining, and the number of colonies was statistically analyzed. $n = 3$. (**D**) Flow cytometry was employed to analyze changes in the cell cycle 48 h after SC13 inhibitor treatment, followed by statistical analysis. $n = 3$. (**E**) Relative mRNA expression levels of *FEN1*, *PCNA*, *BCL-2*, *PIK3CA*, and *Caspase-9* were measured by qRT-PCR 24 h after SC13 inhibitor treatment, using *GAPDH* as the internal reference gene. $n = 3$. (**F**) WB analysis was performed to examine the protein expression levels of FEN1, PCNA, BCL-2, PIK3CA, and Caspase-9 48 h after SC13 inhibitor treatment. Grayscale analysis and statistical evaluation of the WB bands from Panel G were conducted using ImageJ software. $n = 3$. Comparisons with the NC group: *: $P < 0.05$ indicates statistical significance, while **: $P < 0.01$ indicates high statistical significance. Two-independent-samples t-tests was employed to analyze the experimental data in the B-F.

Discussion

In the present study, we conducted a comprehensive proteomic analysis to elucidate the protein expression landscape of SCNECC. This approach enabled us to identify 2333 DEPs. Subsequent in vivo and in vitro experiments provided compelling evidence that FEN1 could potentially serve as a therapeutic target for SCNECC.

At present, owing to the morphological resemblances and partial gene expression profile parallels between SCNECC and small cell lung cancer, patients with SCNECC are treated with the therapeutic regimen for small cell lung cancer. Surgical intervention has demonstrated superior results in patients with stage IB3 - IIA2 SCNECC[3]. Certain scholars have endeavored to enhance SCNECC treatment outcomes by exploring the integration of chemotherapy and radiotherapy or employing a combination of various drugs[18]. Nevertheless, despite these efforts, the dismal prognosis associated with SCNECC underscores the imperative for further investigation and

refinement of its treatment approaches. The TC-YIK cell line, derived from argyrophil small cell carcinoma of the uterine cervix, was successfully established by Hiroshi Ichimura[19]. This cell line is characterized by its ability to express argyrophil granules, neurosecretory granules, neuron-specific enolase, serotonin, and chromogranin, which are hallmark gene expression signatures of SCNECC. Notably, TC-YIK cells harbor multiple copies of integrated HPV DNA and actively transcribe the integrated HPV genome, making it a valuable in vitro experimental model for SCNECC research.

Aberrant gene expression may constitute a pivotal factor in the development of SCNECC. Multiple research groups worldwide have employed sequencing technologies to demonstrate the presence of numerous gene mutations, structural instability of genes, copy number variations (CNVs), and notably high frequencies of PIK3CA and TP53 alterations in SCNECC[13,14,20]. Proteins serve as the executors of cellular functions, and significant alterations in protein expression levels can modulate cellular biological behaviors. Our proteomic analysis revealed that 2168 proteins were upregulated and 165 proteins were downregulated in SCNECC, suggesting that these aberrantly expressed proteins may contribute to the pathogenesis and progression of SCNECC. Furthermore, both GO and KEGG analyses indicated that these DEPs were predominantly enriched in molecular functions and signaling pathways related to DNA replication and RNA transcription, such as mRNA splicing via the spliceosome, RNA splicing, mRNA processing, translational initiation, nuclear-transcribed mRNA catabolic process, RNA binding, mRNA binding, RNA helicase activity, nucleic acid binding, damaged DNA binding, DNA binding, spliceosome, RNA transport, DNA replication, base excision repair, and mismatch repair. These findings suggest a heightened proliferative state in SCNECC, consistent with the results reported by Haifeng Qiu[12]. Given that the inhibition of DNA replication may represent an effective strategy to impede the progression of SCNECC, we selected FEN1, a key molecule in the DNA replication signaling pathway, as the target for further investigation. In addition, the scarcity of SCNECC posed significant challenges in acquiring patient samples. Consequently, we were able to procure only six pairs of cancerous and adjacent non-cancerous tissues from SCNECC patients. The limited sample size inevitably heightened the variability observed in our experimental outcomes. But we employed a combination of in vitro and in vivo experiments to robustly validate the reliability and reproducibility of our experimental findings.

FEN1, a divalent metal-dependent protein endowed with both exonuclease and endonuclease activities, plays a pivotal role in the base excision repair (BER) pathway and is involved in Okazaki fragment maturation during DNA replication[21]. FEN1 is known to play a crucial role in cellular growth and proliferation[22] and elevated FEN1 expression has been implicated as a critical factor in the development of various tumors[23–25]. In this study, proteomic analysis identified FEN1 as a DEP enriched in DNA replication pathways, and IHC confirmed its high expression in SCNECC. To investigate the functional significance of FEN1 in SCNECC, we employed gene silencing to knock down *FEN1* expression in TC-YIK cells. This manipulation significantly inhibited cell proliferation while promoting apoptosis. FEN1 can interact with PCNA, thereby modulating cell proliferation through its influence on DNA replication and repair processes[26,27]. Furthermore, qRT-PCR and WB analyses confirmed that *FEN1* knockdown led to decreased mRNA and protein levels of PCNA, BCL-2, and PIK3CA, with a concurrent increase in Caspase-9 expression in TC-YIK cells, which are widely used to assess the proliferation and apoptotic status of cancer cells. FEN1 not only possesses the ability to interact with PCNA but also has the capacity to modulate PCNA expression levels, thereby governing cell proliferation and other cellular behaviors. In vivo experiments further also validated these findings, demonstrating that knockdown of FEN1 significantly inhibited the growth of SCNECC tumors. These results collectively suggest that FEN1 overexpression may play a pivotal role in the pathogenesis of SCNECC.

FEN1 inhibitors have been developed, and their anti-cancer properties have been experimentally validated across a range of cancer types, such as SC13[21]. In the treatment of cervical cancer, SC13 can significantly improved the effect of paclitaxel and ionizing radiation therapy, suggesting that FEN1 inhibition could be a novel strategy of tumor-targeting therapy for cervical cancer[28,29]. To explore the therapeutic potential of targeting FEN1 in the treatment of SCNECC, we treated TC-YIK cells with SC13. SC13 treatment significantly inhibited cell proliferation and colony formation while promoting apoptosis, mirroring the effects of FEN1 knockdown. Additionally, SC13 reduced the expression of PCNA, BCL-2, and PIK3CA, and increased Caspase-9 expression in TC-YIK cells. Poly (ADP-ribosyl) polymerase-1(PARP1) also is an effective mediator of nucleotide excision repair pathway, which is significantly expressed in various malignant tumors including cervical cancer[30]. PARP inhibitor, a cancer therapy targeting poly(ADP-ribose) polymerase, are the first clinically approved drugs designed to exploit synthetic lethality[31]. The functions of FEN1 and PARP1 bear a resemblance, as both are capable of exerting their influence by interfering with the function of PCNA[32]. From this observation, it becomes evident that FEN1 holds potential as a promising target for targeted therapy in the treatment of SCNECC.

The persistent infection of high-risk HPV is the main cause of cervical cancer, especially HPV16 and HPV18. HPV positivity was observed in over 65.6% of SCNECC cases, with a predominance of HPV18[13,18,33]. All six patients included in this study also tested positive for HPV18. This suggests that HPV18 infection may contribute to the occurrence of SCNECC. HPV DNA replication is an inevitable process of HPV transmission. Consequently, implementing measures to thwart HPV infection, impede HPV DNA replication, and suppress the expression of HPV oncogenes could potentially offer a promising avenue for the prevention and adjunctive treatment of SCNECC. FEN1 plays a key role in the DNA replication process. Treatment targeting FEN1 may inhibit the progression of SCNECC by suppressing HPV DNA replication and the expression of HPV oncogenes. However, Hang Yuan's study reported that HPV-positive SCNECC rely on Myc rather than the E6/E7 viral oncogenes for their oncogenic potential[34]. Therefore, the underlying mechanisms of HPV infection in the initiation and progression of SCNECC warrant further investigation to provide a clearer understanding.

Considering the highly aggressive nature and pronounced propensity for metastasis inherent to SCNECC, early diagnosis assumes paramount importance in optimizing therapeutic outcomes. Liquid biopsies retrieve circulating tumour DNA and circulating tumour RNA released by tumours in addition to circulating tumour

cells[35]. Furthermore, molecular barcoding (MB) of liquid biopsies has been established to be applicable for highly sensitive genomic diagnosis and detection of druggable mutations[36]. This study reveals that elevated FEN1 expression stands out as a distinctive feature within the gene expression profile of SCNECC. Notably, the detection of this heightened FEN1 expression through liquid biopsies holds promise for enabling the early identification of SCNECC, thereby potentially enhancing the prospects for improved therapeutic outcomes.

Conclusions

FEN1 exhibited marked overexpression and played a pivotal role in driving the progression of SCNECC, thereby emerging as a promising therapeutic target for this malignancy. The results of this study provide a solid scientific foundation for elucidating the pathogenesis of SCNECC and for advancing the development of targeted therapeutic strategies.

Materials and methods

Tissue samples, mice and human cell line

Six SCNECC tissue samples were obtained from the Affiliated Cancer Hospital of Shanxi Medical University, with a total of six samples ($n=6$) being utilized for this study. The informed consent was obtained from all subjects. The study protocol received approval from the Ethics Committee of Shanxi Medical University (China). All methods were carried out in accordance with relevant guidelines and regulations and performed in accordance with the Declaration of Helsinki.

BALB/c nude female mice were procured from the Experimental Animal Center of Shanxi Provincial People's Hospital. These mice were housed under specific pathogen-free (SPF) conditions, with a regulated temperature of 25 ± 2 °C, a 12-hour light/dark cycle, and a relative humidity of $50 \pm 10\%$. Throughout the study, the mice were provided with unrestricted access to water and diet. The study protocol received approval from the Experimental Animal Welfare and Ethics Committee of Shanxi Medical University (China). all methods were carried out in accordance with relevant guidelines and regulations All experimental procedures were performed in accordance with ARRIVE guidelines.

TC-YIK, a cell line derived from SCNECC, was acquired from the China Center for Type Culture Collection (located in Wuhan, China). These cells were cultured in Dulbecco's modified Eagle's medium (DMEM) (Catalog Number: 8122691, supplied by Gibco, Thermo Fisher, USA), supplemented with 10% fetal bovine serum (Catalog Number: 10100147, also from Gibco, Thermo Fisher, USA) and 1% penicillin/streptomycin. All cell cultures were maintained in an incubator with a 5% CO_2 atmosphere at a temperature of 37 °C.

Sample preparation and mass spectrometry

The pathology specimens of SCNECC are preserved as formalin-fixed, paraffin-embedded (FFPE) blocks. Protein extraction was carried out using FFPE samples obtained from six patients. Initially, the samples were sectioned into 5 μm-thick slices using a microtome and then dried for 16 h on a paraffin extender at 44 °C. Following deparaffinization, the slides were allowed to dry at room temperature for one hour. Each sample was subsequently suspended in 100 μL of 0.1 mol/L NH_4HCO_3 containing 30% (v/v) CH_3CN and homogenized three times (Speed: 7800 rpm, Cycle: 3×20 s, Pause: 30 s) using a lysis and homogenization system (Bertin Technologies SAS, France). The samples were then centrifuged at $10,000 \times g$ for 1 min at 4 °C. To eliminate formalin cross-links, the samples were heated at 95 °C for 90 min and centrifuged again at 4 °C for 1 min at $10,000 \times g$. Protein concentration was measured using a Qubit® 2.0 Fluorometer (Qubit Protein Assay kits, Thermo Fisher Scientific, Waltham, MA).

For LC-MS/MS analysis, peptides were separated using a 120-minute gradient elution at a flow rate of 0.300 μL/min with a Thermo-Dionex Ultimate 3000 HPLC system, which was directly interfaced with the Thermo Orbitrap Fusion mass spectrometer. The analytical column was a self-made fused silica capillary column (75 μm internal diameter, 150 mm length; Upchurch, Oak Harbor, WA) packed with C-18 resin (300 A, 5 μm; Varian, Lexington, MA). Mobile phase A consisted of 0.1% formic acid, and mobile phase B consisted of 100% acetonitrile and 0.1% formic acid. The Orbitrap Fusion mass spectrometer was operated in data-dependent acquisition mode using Xcalibur 3.0 software. Each run included a single full-scan mass spectrum in the Orbitrap (350–1550 m/z, 120,000 resolution) followed by 3-second data-dependent MS/MS scans in an Ion Routing Multipole at 30% normalized collision energy (HCD). The MS/MS spectra from each LC-MS/MS run were searched against the selected database using the Proteome Discovery searching algorithm (version 1.4).

GO and KEGG pathway analysis

GO is employed to conduct an enrichment analysis that encompasses the cellular components, biological processes, and molecular functions associated with the selected proteins. KEGG serves as a comprehensive database utilized to elucidate the functionalities and biochemical pathways involving the chosen proteins[37]. RStudio was utilized to execute both GO and KEGG pathway analyses via the "clusterProfiler" package[38,39]. Additionally, data visualization was accomplished using the "GOplot" package.

IHC analysis

Section (4 μm) of SCNECC tissues and adjacent normal cervical tissues were subjected to dewaxing and rehydration processes. This was followed by an antigen retrieval procedure, which involved the use of citrate buffer at pH 6.0 and heating at 95 °C for 15 min. For the staining of Ki67, P16, AE1/AE3, SYN, and FEN1, the sections were immersed in 3% hydrogen peroxide (H_2O_2) for 15 min and then incubated overnight at 4 °C with rabbit antibodies specific to these proteins (Ki67, catalog number: 27309-1-AP, dilution 1:16000; P16, catalog number: 10883-1-AP, dilution 1:2000; AE1/AE3, catalog number: 26411-1-AP, dilution 1:3000; SYN, catalog

number: 17785-1-AP, dilution 1:2000; FEN1, catalog number: 14768-1-AP, dilution 1:2000; all from Proteintech, USA). Matched rabbit non-immune IgG was used as a negative control. Subsequently, the sections were treated with horseradish peroxidase (HRP)-conjugated anti-rabbit IgG (PV-6001; Zymed Laboratories, China) and incubated for 20 min at 37 °C. The proteins were visualized using 3,3'-diaminobenzidine tetrahydrochloride and counterstained with hematoxylin.

The stained sections were scored by two observers who were blinded to the patients' clinical outcomes, according to the following criteria: Cells with less than 10% staining were scored as negative staining (1); cells with 10–49% staining were assigned a score of (2); cells with 50–74% staining were scored as (3); and cells with 75–100% staining were scored as (4). The staining color was scored as follows: no staining (0), light-yellow particles (1), brown-yellow particles (2), and brown particles (3). The final score was calculated as the product of the staining number score and the staining color score[40]. Discrepancies between the observers were observed in less than 10% of the slides examined, and consensus was reached upon further review.

Cell transfection

Cells were seeded in 6-well plates and allowed to proliferate until they entered the logarithmic growth phase. Subsequently, negative control (NC), FEN1 siRNA, and proliferating cell nuclear antigen (PCNA) siRNA were introduced into the cells using Lipofectamine 2000 reagent (Catalog Number: 11668019, Invitrogen, Carlsbad, CA, USA), adhering to the manufacturer's guidelines. The sequences of these siRNAs were meticulously designed and synthesized by GenePharma (Shanghai, China), with the following details: NC: Sense: UUCUCCGAACGU GUCACGUTT, Antisense: ACGUGACACGUUCGGAGAATT; FEN1 siRNA: Sense:: GCCCGUGUAUGUCU UUGAUTT, Antisense: AUCAAAGACAUACACGGGCTT; PCNA siRNA: Sense: AACCUCACCAGUAUGUC CATT, Antisense: UGGACAUACUGGUGAGGUUTT.

Transfection was conducted for a duration of 6 h, after which the medium was replaced with complete medium containing 10% fetal bovine serum to halt the transfection process. The cells were then further cultivated and harvested at either 24–48 h post-transfection for subsequent experimental analyses.

In vitro Cell proliferation assays

CCK-8 assay (Dojindo Laboratories, Japan) accurately quantified proliferative responses and has been used in both infection biology and oncology contexts[41–43]. The proliferative capacity of TC-YIK cells was evaluated using a CCK-8, in strict accordance with the manufacturer's instructions, following transfection with NC, FEN1 siRNA, or PCNA siRNA. Each treatment group was allocated five wells for this assay. The experiment was independently replicated three times, and the results are presented as the absorbance values measured at 450 nm for the NC, FEN1 siRNA, or PCNA siRNA groups.

Colony formation assay

Approximately 500 TC-YIK cells were seeded into small culture dishes and incubated at 37 °C in a humidified incubator maintained at 5% CO_2. The culture medium was refreshed every two days. Following a 14-day incubation period, the cells were gently rinsed with phosphate-buffered saline (PBS), fixed in methanol for 15 min, and subsequently stained with crystal violet for an additional 15 min. Colonies comprising a minimum of 50 cells were enumerated using Image Processing and Analysis in Java (ImageJ) software (version number:1.54 g, URL link: https://imagej.net/ij/download.html, National Institutes of Health, USA).

Flow cytometry analysis

Cell apoptosis was assessed via flow cytometry[44,45] utilizing an AnnexinV-FITC/PI Apoptosis Kit (MeilunBio, China). For sample preparation, 5 µL of Annexin V-FITC and 10 µL of propidium iodide (PI) were added to detect phosphatidylserine (PS) exposure on the external leaflet of the plasma membrane. Following a 15-minute incubation in a light-protected environment, the samples were quantified using flow cytometry (BD Biosciences, San Jose, CA, USA). Each treatment was performed in duplicate, and the entire experiment was executed in triplicate.

Transfected TC-YIK cells were gently centrifuged at 2000 g for 5 min at 25 °C. The cells were subsequently resuspended in PBS to achieve a density of 1×10^5 cells/mL. After thorough mixing with 75% ethanol, the cells were incubated for 12 h at 4 °C. The cells were then washed with PBS and centrifuged at 2000 g for 3 min. Thereafter, 400 µL of the cell cycle detection reagent from the Tali™ Cell Cycle Kit (Thermo Fisher Scientific) was added to resuspend the cells, which were then subjected to further flow cytometric analysis.

qRT-PCR

qRT-PCR was conducted following the previously described protocol[42,46]. In brief, RNA was extracted using TRIzol reagent (Catalog Number: 15596026, Invitrogen, USA), and complementary DNA (cDNA) was synthesized from approximately 2 µg of total RNA utilizing Moloney murine leukemia virus reverse transcriptase (TaKaRa Bio, Otsu, Japan) along with oligo-(dT)$_{18}$ primers. qRT-PCR was carried out using a StepOnePlus™ Real-Time PCR System (Applied Biosystems, Thermo Fisher Scientific, USA) with SYBR Premix Ex Taq II (TaKaRa Bio, Otsu, Japan). Glyceraldehyde-3-phosphate dehydrogenase (GAPDH) served as the internal control gene to normalize the mRNA expression levels. The thermal cycling conditions were as follows: an initial activation step at 95 °C for 30 s, succeeded by 40 cycles of denaturation at 95 °C for 5 s and annealing/extension at 60 °C for 34 s. The primer sequences were designed and synthesized by Sangon Biotech (Shanghai, China) (Supplementary Table 4). Each sample was analyzed in triplicate. Relative RNA quantification was performed using the $2^{-\Delta\Delta Ct}$ method.

WB analysis

WB analysis was conducted in accordance with previously established experimental protocols[17,46]. In brief, total protein lysates were extracted using RIPA lysis and extraction buffer (Catalog Number: AR0102, Biological Technology Co., Ltd., China). Protein concentrations were determined utilizing the BCA Protein Assay Kit (Catalog Number: AR1189, Biological Technology Co., Ltd., China). Proteins were resolved by sodium dodecyl sulfate-polyacrylamide gel electrophoresis (SDS-PAGE) and subsequently transferred onto polyvinylidene fluoride (PVDF) membranes (Millipore, Billerica, MA, USA). The membranes were blocked for 1 h at room temperature in 5% (w/v) nonfat dried milk and then incubated with primary antibodies specific for FEN1 (Catalog Number: 14768-1-AP; 1:2000, Proteintech Group, China), PCNA (Catalog Number: 10205-2-AP; 1:10000, Proteintech Group, China), Caspase-9 (Catalog Number: 10380-1-AP; 1:300, Proteintech, China), BCL-2 (Catalog Number: 12789-1-AP; 1:9000, Proteintech Group, China), PIK3CA (Catalog Number: PB0351; 1:1000, Biological Technology Co., Ltd., China), and GAPDH (Catalog Number: AP0063, Bioworld Technology, Inc., China). An enhanced chemiluminescence kit (Catalog Number: AR1171, Boster Biological Technology Co., Ltd., China) was employed for band visualization. Finally, automatic exposure was carried out using a chemiluminescence gel imaging system (FluorChem E, ProteinSimple, USA). The grayscale values of the exposed bands were quantified and analyzed using ImageJ software. Each sample was analyzed in triplicate.

Animal experiments

The mice were randomly allocated into two distinct groups, comprising five animals each. To investigate the impact of FEN1 in SCNECC, 5×10^6 TC-YIK cells were injected into the right axillae of the nude mice. Upon the tumor volume surpassing 50 mm³, 5 nmol of either in vivo NC siRNA or in vivo FEN1 siRNA (GenePharma, Shanghai, China) was administered into the tumor every 2 days for a total of five injections. Tumor volumes were measured every 2 days and calculated using the formula: $(L \times W^2)/2$, where L represents the longest diameter and W represents the shortest diameter perpendicular to L. The mice were euthanized through cervical vertebrae dislocation, after which the tumor tissues were extracted for subsequent analysis. All animal procedures adhered to the guidelines for the care and use of experimental animals established by the National Cancer Center.

FEN1 inhibitor treatment

Cells were seeded into a 96-well plate. FEN1-IN-SC13 (Catalog Number: HY-145758, MedChemExpress, USA), a widely utilized FEN1 inhibitor in scientific research, was added to the cell culture medium, and the cells were subsequently cultured further. Two concentration groups were established: a 0 µM group (control) and a 40 µM group (experimental), with triplicate wells for each group. Following culture for 0 h, 24 h, 48 h and 72 h, the cellular functions were evaluated.

Statistical analysis

Two-way analysis of variance (ANOVA) and two-independent-samples t-tests were employed to analyze the experimental data, with statistical significance denoted by $*P < 0.05$ and $**P < 0.01$. Statistical analyses were conducted using GraphPad Prism (version 9.0.0, GraphPad Software). All results are presented as the means ± standard deviations (SDs).

Data availability

All data needed to evaluate the conclusions in the paper are present in the paper and/or the Supplementary Materials.

References

1. Bray, F. et al. Global cancer statistics 2022: GLOBOCAN estimates of incidence and mortality worldwide for 36 cancers in 185 countries. *CA Cancer J. Clin.* **74**, 229–263. https://doi.org/10.3322/caac.21834 (2024).
2. Siegel, R. L., Giaquinto, A. N. & Jemal, A. Cancer statistics, 2024. *CA Cancer J. Clin.* **74**, 12–49. https://doi.org/10.3322/caac.21820 (2024).
3. Chu, T. et al. The prognosis of patients with small cell carcinoma of the cervix: A retrospective study of the SEER database and a Chinese multicentre registry. *Lancet Oncol.* **24**, 701–708. https://doi.org/10.1016/s1470-2045(23)00185-7 (2023).
4. Atienza-Amores, M., Guerini-Rocco, E., Soslow, R. A., Park, K. J. & Weigelt, B. Small cell carcinoma of the gynecologic tract: A multifaceted spectrum of lesions. *Gynecol. Oncol.* **134**, 410–418. https://doi.org/10.1016/j.ygyno.2014.05.017 (2014).
5. Lin, L. M. et al. Prognostic factors and treatment comparison in small cell neuroendocrine carcinoma of the uterine cervix based on population analyses. *Cancer Med.* **9**, 6524–6532. https://doi.org/10.1002/cam4.3326 (2020).
6. Salvo, G., Gonzalez, M. A., Gonzales, N. & Frumovitz, M. Updates and management algorithm for neuroendocrine tumors of the uterine cervix. *Int. J. Gynecol. Cancer Off. J. Int. Gynecol. Cancer Soc.* **29**, 986–995. https://doi.org/10.1136/ijgc-2019-000504 (2019).
7. Sonkin, D., Thomas, A. & Teicher, B. A. Cancer treatments: Past, present, and future. *Cancer Genet.* 286–287. https://doi.org/10.1016/j.cancergen.2024.06.002 (2024).
8. Xiao, Y. & Yu, D. Tumor microenvironment as a therapeutic target in cancer. *Pharmacol. Ther.* **221**, 107753. https://doi.org/10.1016/j.pharmthera.2020.107753 (2021).
9. Liu, H. & Dilger, J. P. Different strategies for cancer treatment: Targeting cancer cells or their neighbors? *Chin. J. Cancer Res.* **37**, 289–292. https://doi.org/10.21147/j.issn.1000-9604.2025.02.12 (2025).
10. Schechter, A. L. et al. The Neu oncogene: An erb-B-related gene encoding a 185,000-Mr tumour antigen. *Nature* **312**, 513–516. https://doi.org/10.1038/312513a0 (1984).
11. Telang, M. J. R., Soni, B., Khalife, A. & G. & Overview of perspectives on cancer, newer therapies, and future directions. *Oncol. Transl. Med.* **10**, 105–109. https://doi.org/10.1097/ot9.0000000000000039 (2024).

12. Qiu, H., Su, N., Wang, J., Yan, S. & Li, J. Quantitative proteomics analysis in small cell carcinoma of cervix reveals novel therapeutic targets. *Clin. Proteom.* **20**, 18. https://doi.org/10.1186/s12014-023-09408-x (2023).

13. Wang, W. et al. Whole exome sequencing identifies common mutational landscape of cervix and endometrium small cell neuroendocrine carcinoma. *Front. Oncol.* **13**, 1182029. https://doi.org/10.3389/fonc.2023.1182029 (2023).

14. Pan, B. et al. Multiomics sequencing and immune microenvironment characteristics define three subtypes of small cell neuroendocrine carcinoma of the cervix. *J. Pathol.* https://doi.org/10.1002/path.6290 (2024).

15. Kwon, Y. W. et al. Application of proteomics in cancer: Recent trends and approaches for biomarkers discovery. *Front. Med. (Lausanne).* **8**, 747333. https://doi.org/10.3389/fmed.2021.747333 (2021).

16. Mani, D. R. et al. Cancer proteogenomics: Current impact and future prospects. *Nat. Rev. Cancer.* **22**, 298–313. https://doi.org/10.1038/s41568-022-00446-5 (2022).

17. Liu, H. et al. The voltage-gated sodium channel β3 subunit modulates C6 glioma cell motility independently of channel activity. *Biochim. et Biophys. Acta. Mol. Basis Dis.* **1871**, 167844 (2025). https://doi.org/10.1016/j.bbadis.2025.167844

18. Bellone, S. et al. Integrated mutational landscape analysis of poorly differentiated high-grade neuroendocrine carcinoma of the uterine cervix. *Proc. Natl. Acad. Sci. U S A.* **121**, e2321898121. https://doi.org/10.1073/pnas.2321898121 (2024).

19. Ichimura, H. et al. Establishment and characterization of a new cell line TC-YIK originating from argyrophil small cell carcinoma of the uterine cervix integrating HPV16 DNA. *Cancer* **67**, 2327–2332. 10.1002/1097-0142(19910501)67:9<2327::AID-CNCR2820670919>3.0.CO;2-F (1991).

20. Pei, X. et al. The next generation sequencing of cancer-related genes in small cell neuroendocrine carcinoma of the cervix. *Gynecol. Oncol.* **161**, 779–786. https://doi.org/10.1016/j.ygyno.2021.04.019 (2021).

21. Yang, F., Hu, Z. & Guo, Z. Small-molecule inhibitors targeting FEN1 for cancer therapy. *Biomolecules* **12** (2022). https://doi.org/10.3390/biom12071007

22. Lieber, M. R. The FEN-1 family of structure-specific nucleases in eukaryotic DNA replication, recombination and repair. *Bioessays* **19**, 233–240. https://doi.org/10.1002/bies.950190309 (1997).

23. Zhang, K. et al. Overexpression of flap endonuclease 1 correlates with enhanced proliferation and poor prognosis of Non-Small-Cell lung Cancer. *Am. J. Pathol.* **188**, 242–251. https://doi.org/10.1016/j.ajpath.2017.09.011 (2018).

24. Zhang, Y. et al. Upregulation of FEN1 is associated with the tumor progression and prognosis of hepatocellular carcinoma. *Dis Markers* **2514090** (2020). https://doi.org/10.1155/2020/2514090 (2020).

25. Wang, S. et al. Down-regulation of DNA key protein-FEN1 inhibits OSCC growth by affecting immunosuppressive phenotypes via IFN-γ/JAK/STAT-1. *Int. J. Oral Sci.* **15**, 17. https://doi.org/10.1038/s41368-023-00221-8 (2023).

26. Zheng, L. et al. Fen1 mutations that specifically disrupt its interaction with PCNA cause aneuploidy-associated cancer. *Cell. Res.* **21**, 1052–1067. https://doi.org/10.1038/cr.2011.35 (2011).

27. Tian, Y., Li, N., Li, Q. & Gao, N. Structural insight into Okazaki fragment maturation mediated by PCNA-bound FEN1 and RNaseH2. *EMBO J.* **44**, 484–504. https://doi.org/10.1038/s44318-024-00296-x (2025).

28. He, L. et al. Synergistic antitumor effect of combined Paclitaxel with FEN1 inhibitor in cervical cancer cells. *DNA Repair. (Amst).* **63**, 1–9. https://doi.org/10.1016/j.dnarep.2018.01.003 (2018).

29. Li, J. L. et al. FEN1 inhibitor increases sensitivity of radiotherapy in cervical cancer cells. *Cancer Med.* **8**, 7774–7780. https://doi.org/10.1002/cam4.2615 (2019).

30. Mann, M., Singh, V. P. & Kumar, L. Cervical cancer: A Tale from HPV infection to PARP inhibitors. *Genes Dis.* **10**, 1445–1456. https://doi.org/10.1016/j.gendis.2022.09.014 (2023).

31. Lord, C. J. & Ashworth, A. PARP inhibitors: Synthetic lethality in the clinic. *Science* **355**, 1152–1158. https://doi.org/10.1126/science.aam7344 (2017).

32. Aleksandrov, R. et al. Protein dynamics in complex DNA lesions. *Mol. Cell.* **69**, 1046–1061. https://doi.org/10.1016/j.molcel.2018.02.016 (2018). e1045.

33. Takayanagi, D. et al. Comparative analysis of genetic alterations, HPV-Status, and PD-L1 expression in neuroendocrine carcinomas of the cervix. *Cancers (Basel).* **13**. https://doi.org/10.3390/cancers13061215 (2021).

34. Yuan, H. et al. HPV positive neuroendocrine cervical cancer cells are dependent on Myc but not E6/E7 viral oncogenes. *Sci. Rep.* **7**, 45617. https://doi.org/10.1038/srep45617 (2017).

35. Jahangiri, L. Updates on liquid biopsies in neuroblastoma for treatment response, relapse and recurrence assessment. *Cancer Genet.* 288–289. https://doi.org/10.1016/j.cancergen.2024.09.001 (2024).

36. Ohyama, H. et al. Development of a molecular barcode detection system for pancreaticobiliary malignancies and comparison with next-generation sequencing. *Cancer Genet.* 280–281. https://doi.org/10.1016/j.cancergen.2023.12.002 (2024).

37. Kanehisa, M., Furumichi, M., Sato, Y., Matsuura, Y. & Ishiguro-Watanabe, M. KEGG: Biological systems database as a model of the real world. *Nucleic Acids Res.* **53**, D672–d677. https://doi.org/10.1093/nar/gkae909 (2025).

38. Liu, H. & Weng, J. A comprehensive bioinformatic analysis of cyclin-dependent kinase 2 (CDK2) in glioma. *Gene* **822**, 146325. https://doi.org/10.1016/j.gene.2022.146325 (2022).

39. Liu, H. & Tang, T. A bioinformatic study of IGFBPs in glioma regarding their diagnostic, prognostic, and therapeutic prediction value. *Am. J. Transl. Res.* **15**, 2140–2155 (2023).

40. Guo, Z. et al. TELO2 induced progression of colorectal cancer by binding with RICTOR through mTORC2. *Oncol. Rep.* **45**, 523–534. https://doi.org/10.3892/or.2020.7890 (2021).

41. Ou, L. et al. Chebulinic acid isolated from aqueous extracts of Terminalia chebula Retz inhibits Helicobacter pylori infection by potential binding to Cag A protein and regulating adhesion. *Front. Microbiol.* **15**, 1416794. https://doi.org/10.3389/fmicb.2024.1416794 (2024).

42. Wu, Z. et al. Icaritin induces MC3T3-E1 subclone14 cell differentiation through Estrogen receptor-mediated ERK1/2 and p38 signaling activation. *Biomed. Pharmacotherapy Biomedecine Pharmacotherapie.* **94**, 1–9. https://doi.org/10.1016/j.biopha.2017.07.071 (2017).

43. Liu, H., Dilger, J. P. & Lin, J. Effects of local anesthetics on cancer cells. *Pharmacol. Ther.* **212**, 107558. https://doi.org/10.1016/j.pharmthera.2020.107558 (2020).

44. Liu, H., Dilger, J. P. & Lin, J. The role of transient receptor potential melastatin 7 (TRPM7) in cell viability: A potential target to suppress breast Cancer cell cycle. *Cancers (Basel).* **12**. https://doi.org/10.3390/cancers12010131 (2020).

45. Li, R. et al. Effects of local anesthetics on breast cancer cell viability and migration. *BMC Cancer.* **18**, 666. https://doi.org/10.1186/s12885-018-4576-2 (2018).

46. Liu, J. et al. Upregulation of miR-205 induces CHN1 expression, which is associated with the aggressive behaviour of cervical cancer cells and correlated with lymph node metastasis. *BMC Cancer.* **20**, 1029. https://doi.org/10.1186/s12885-020-07478-w (2020).

Acknowledgements

Author contributions

Funding

Declarations

Competing interests

The authors declare no competing interests.

Ethics approval

Ethical approval was provided by the Ethics Committee of the Shanxi Medical University.

Informed consent

Each patient provided informed consent for the use of the samples in this study.

Additional information

Supplementary Information The online version contains supplementary material available at https://doi.org/10.1038/s41598-025-12892-w.

Correspondence and requests for materials should be addressed to J.L. or H.M.

Reprints and permissions information is available at www.nature.com/reprints.

Publisher's note Springer Nature remains neutral with regard to jurisdictional claims in published maps and institutional affiliations.